Supplementary Information

Hopping Dynamics of a Tracer Particle Confined in a Fluctuating Lattice

Seonghui Kim,[ab] Yeonho Song,[ab] Bong June Sung,[*c] Shinji Saito,[*de] and Jun Soo Kim[*ab]

[a] *Department of Chemistry and Nanoscience, Ewha Womans University, Seoul 03760, Republic of Korea, E-mail: jkim@ewha.ac.kr*

[a] *Institute for Multiscale Matter and Systems, Ewha Womans University, Seoul 03760, Republic of Korea*

[c] *Department of Chemistry and Institute of Biological Interfaces, Sogang University, Seoul 04107, Republic of Korea, E-mail: bjsung@sogang.ac.kr*

[d] *Institute for Molecular Science, Myodaiji, Okazaki, Aichi 444-8585, Japan, E-mail: shinji@ims.ac.jp*

[e] *The Graduate University for Advanced Studies (SOKENDAI), Myodaiji, Okazaki, Aichi 444-8585, Japan*

Contents

Figure S7. Probability distributions of the hop functions plotted on a semi-logarithmic scale to determine threshold values without direct tracking of hopping events for $k_f = 40\ k_B T/\sigma^2$.

Figure S8. Probability distribution of the residence time, t_R, defined as the time interval between consecutive hopping events of $h(t)$, $h_1(t)$, and $h_2(t)$, compared with that from direct tracer tracking.

Figure S9. Comparison of the distribution of the tracer along the *y*-direction for the restraining constant k_y= 0.5, 1, 2, 3, 4 and 5 $k_B T/\sigma^2$ at $x = 0$.

Figure S10. Comparison of the potential of mean force (PMF) profiles of the tracer along the x-axis under different restraining conditions: free along the y-axis ($k_y = 0$), restrained along the y-axis with the y-directional force constant of k_y= 3, 10, 50 $k_B T/\sigma^2$, and fixed along y-axis.

Figure S11. Comparisons of the time-local diffusion coefficient $D_t(t)$ with the directly tracked tracer trajectory for various combinations of the lag time Δ and the analysis window t_w at $k_f = 40\ k_B T/\sigma^2$.

Figure S12. Validation of the time-local diffusion coefficient $D_t(t)$ for accurate identification of hopping events at $k_f = 40\ k_B T/\sigma^2$.

Figure S13. Calculation of residence time using Kramers' theory.

$k_\mathrm{f}\ (k_\mathrm{B}T/\sigma^2)$	4	10	20	40	60	100
$h^*\ (\sigma^2)$	0.95	0.90	0.90	0.90	1.05	1.05
$h_1^*\ (\sigma)$	1.65	1.60	1.55	1.50	1.50	1.45
$h_2^*\ (\sigma)$	1.75	1.75	1.75	1.75	1.60	1.60

Table S1. Threshold values for hop functions, h^*, h_1^*, and h_2^*. The threshold values represent the minimum criteria above which hopping events are identified. They were chosen by comparing hop-function results with direct tracking and selecting the value that yielded the fewest inconsistent identifications.

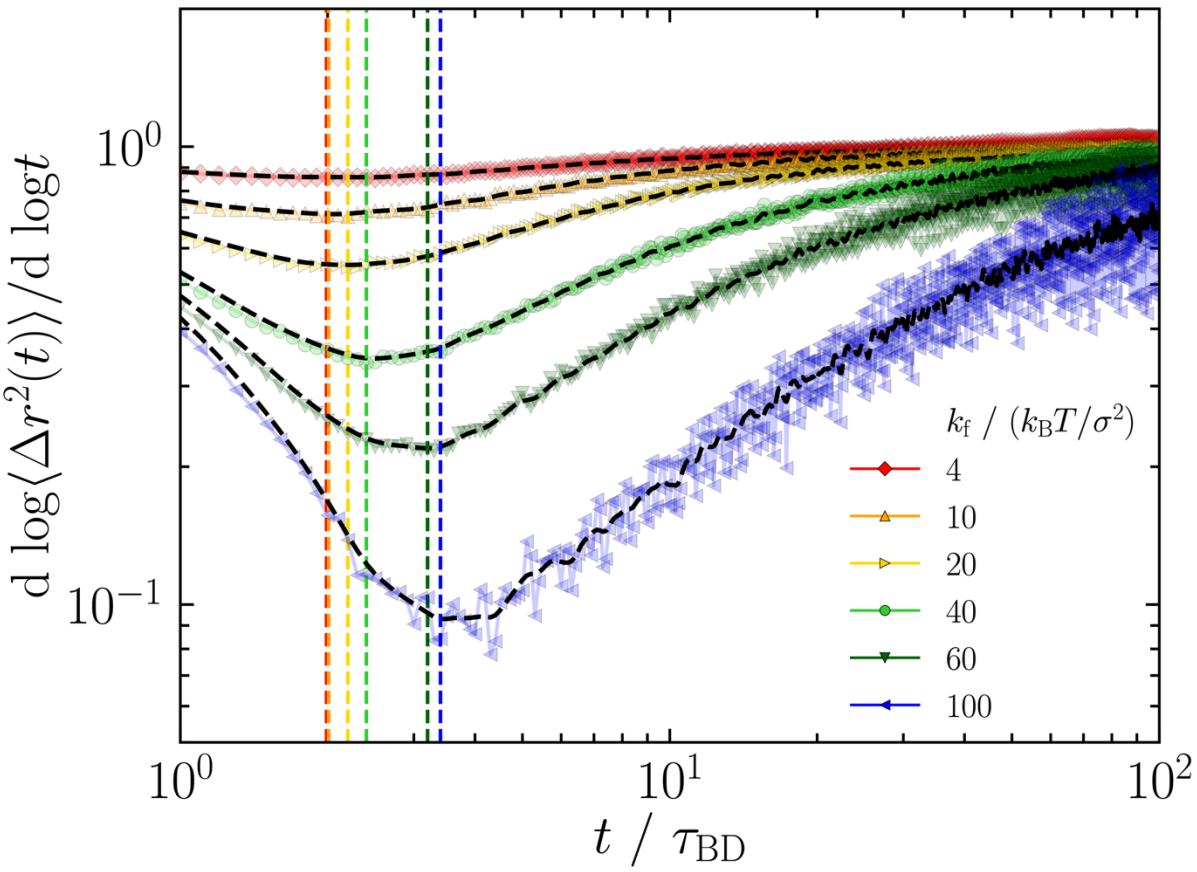

Figure S1. Comparisons of the logarithmic derivative of the mean square displacement (MSD) with respect to time obtained for various values of k_f (in unit of k_BT/σ^2). The vertical dashed lines indicate the values of Δt for each k_f, as presented in Table 1 of the main text. These values were determined by finding the time corresponding to the minimum of d log $\langle \Delta r^2(t) \rangle$/d log t, which was computed from MSD data smoothed using a Gaussian filter (σ = 2.0). The resulting Δt values were rounded such that the first decimal place is even, ensuring compatibility with the 0.2-interval used for averaging.

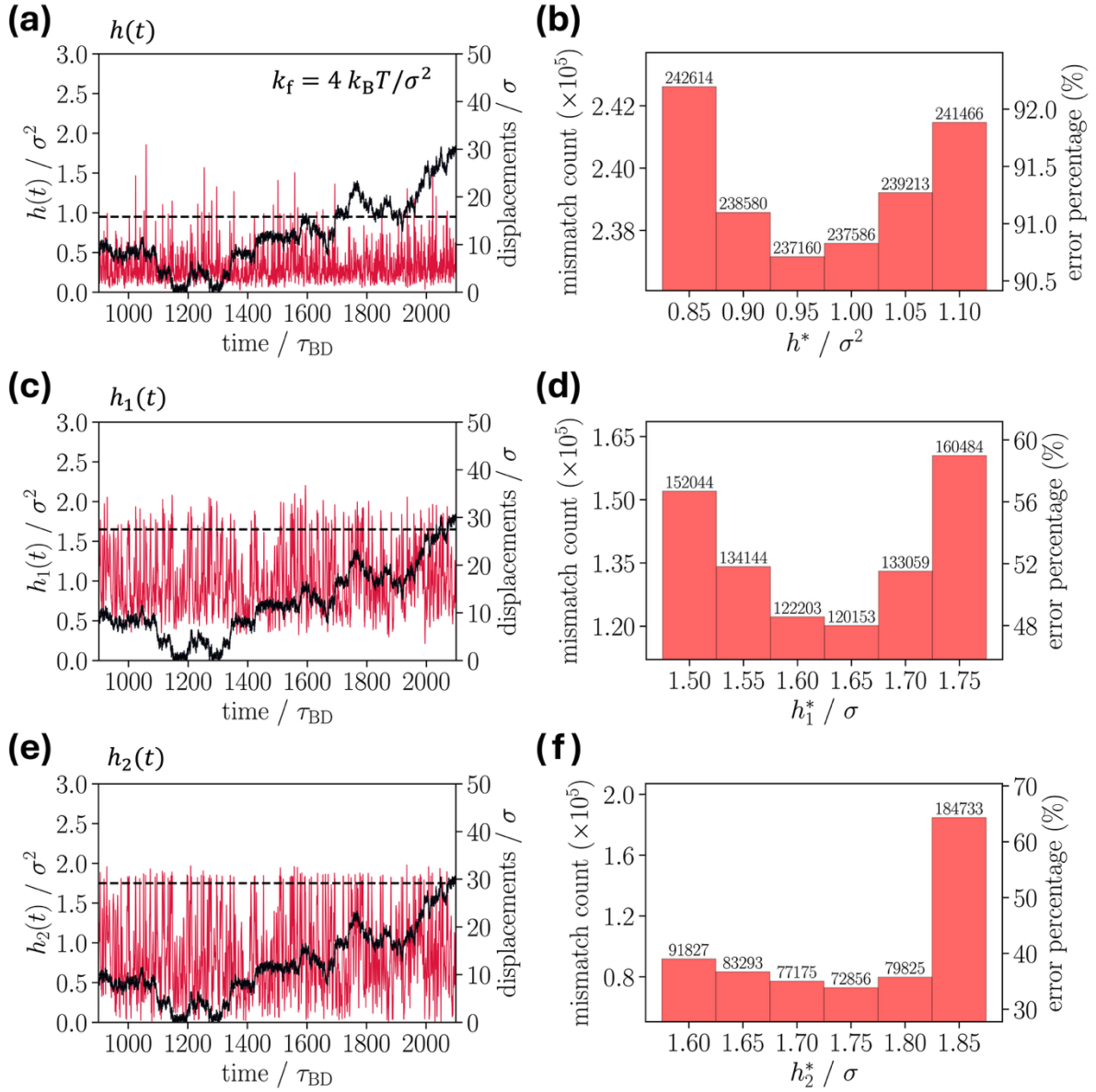

Figure S2. Validation of the hop functions for accurate identification of hopping events for $k_f = 4\ k_B T/\sigma^2$. ((a), (c), (e)) Comparisons of $h(t)$, $h_1(t)$, and $h_2(t)$ (red curves, plotted against the left y-axis) with the directly tracked tracer trajectory (black curve, plotted against the right y-axis) over the simulation period from 900 τ_{BD} to 2,100 τ_{BD} for $k_f = 4\ k_B T/\sigma^2$. Horizontal dashed lines indicate the optimized threshold values for each hop function (see Table S1), used to identify hopping events. ((b), (d), (f)) The number of inconsistent identifications of hopping events as a function of threshold values for $h(t)$, $h_1(t)$, and $h_2(t)$. The total number of hopping events directly identified from the entire simulation trajectory ($4\times10^6\ \tau_{BD}$) for $k_f = 4\ k_B T/\sigma^2$, is 262,301. The error percentage is calculated as the mismatch count divided by this total, multiplied by 100.

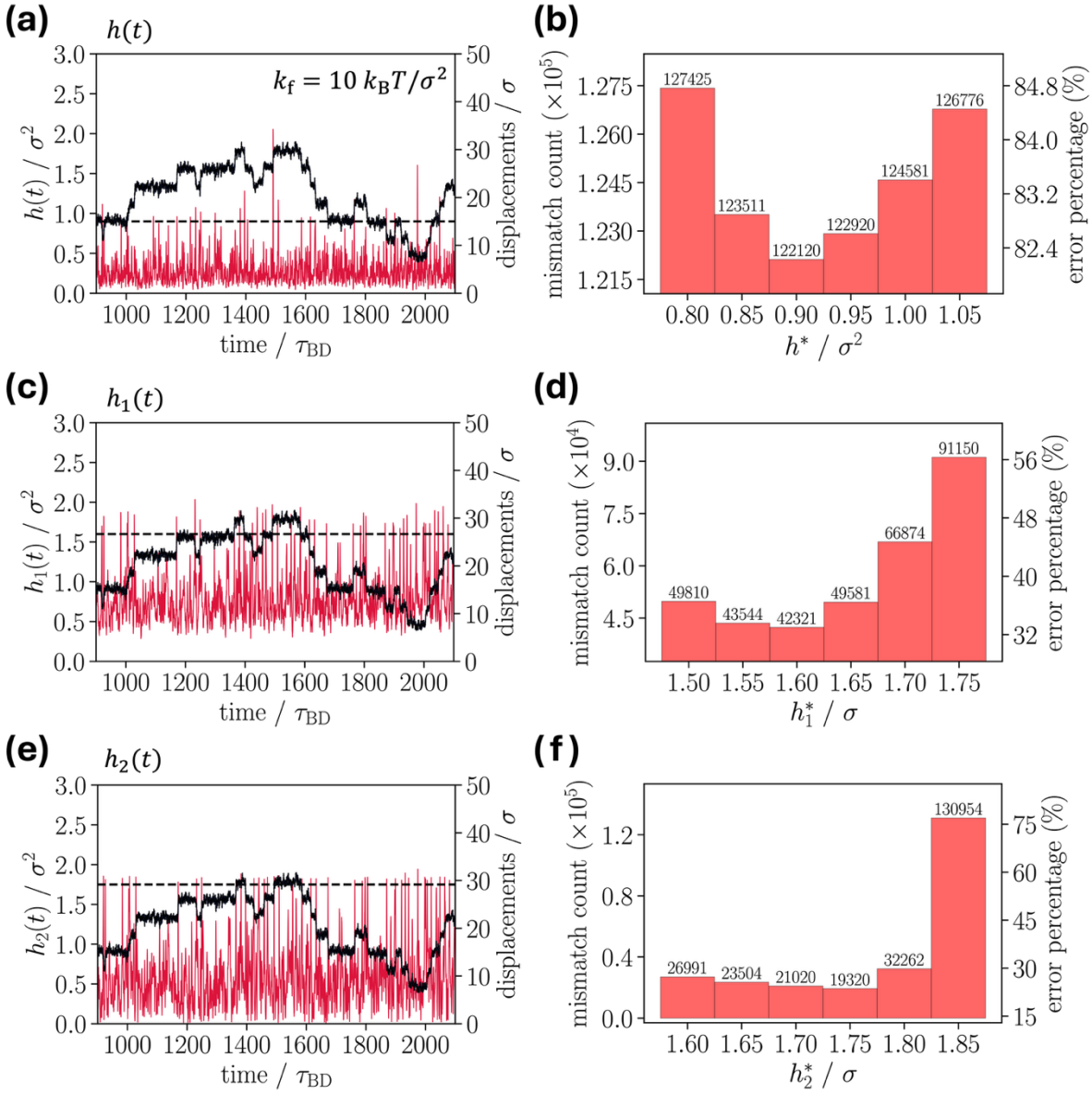

Figure S3. Validation of the hop functions for accurate identification of hopping events for $k_f = 10\ k_B T/\sigma^2$. ((a), (c), (e)) Comparisons of $h(t)$, $h_1(t)$, and $h_2(t)$ (red curves, plotted against the left y-axis) with the directly tracked tracer trajectory (black curve, plotted against the right y-axis) over the simulation period from 900 τ_{BD} to 2,100 τ_{BD} for $k_f = 10\ k_B T/\sigma^2$. Horizontal dashed lines indicate the optimized threshold values for each hop function (see Table S1), used to identify hopping events. ((b), (d), (f)) The number of inconsistent identifications of hopping events as a function of threshold values for $h(t)$, $h_1(t)$, and $h_2(t)$. The total number of hopping events directly identified from the entire simulation trajectory ($4\times10^6\ \tau_{BD}$) for $k_f = 10\ k_B T/\sigma^2$, is 149,434. The error percentage is calculated as the mismatch count divided by this total, multiplied by 100.

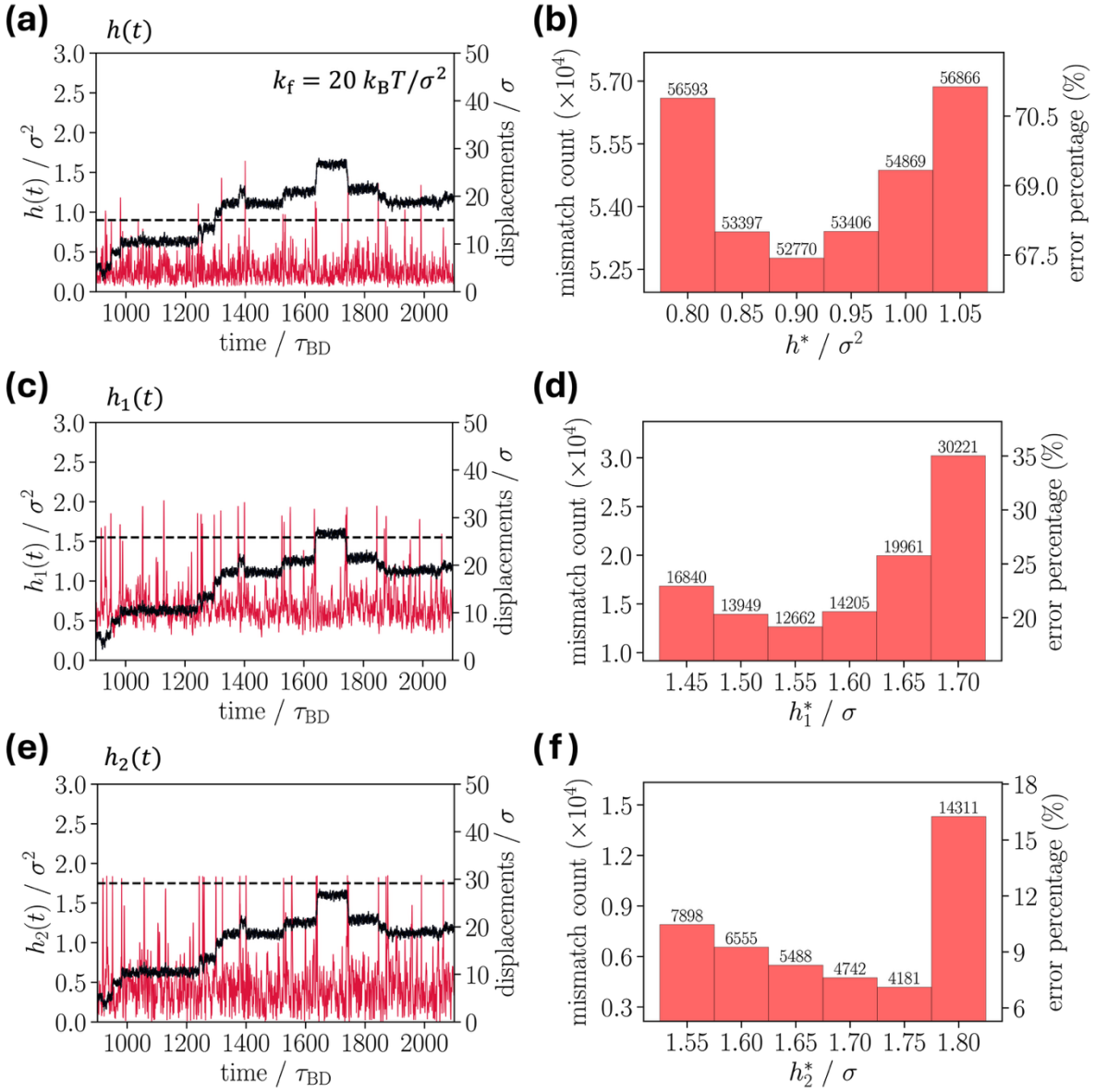

Figure S4. Validation of the hop functions for accurate identification of hopping events for $k_f = 20\ k_B T/\sigma^2$. ((a), (c), (e)) Comparisons of $h(t)$, $h_1(t)$, and $h_2(t)$ (red curves, plotted against the left y-axis) with the directly tracked tracer trajectory (black curve, plotted against the right y-axis) over the simulation period from 900 τ_{BD} to 2,100 τ_{BD} for $k_f = 20\ k_B T/\sigma^2$. Horizontal dashed lines indicate the optimized threshold values for each hop function (see Table S1), used to identify hopping events. ((b), (d), (f)) The number of inconsistent identifications of hopping events as a function of threshold values for $h(t)$, $h_1(t)$, and $h_2(t)$. The total number of hopping events directly identified from the entire simulation trajectory ($4\times10^6\ \tau_{BD}$) for $k_f = 20\ k_B T/\sigma^2$, is 79,118. The error percentage is calculated as the mismatch count divided by this total, multiplied by 100.

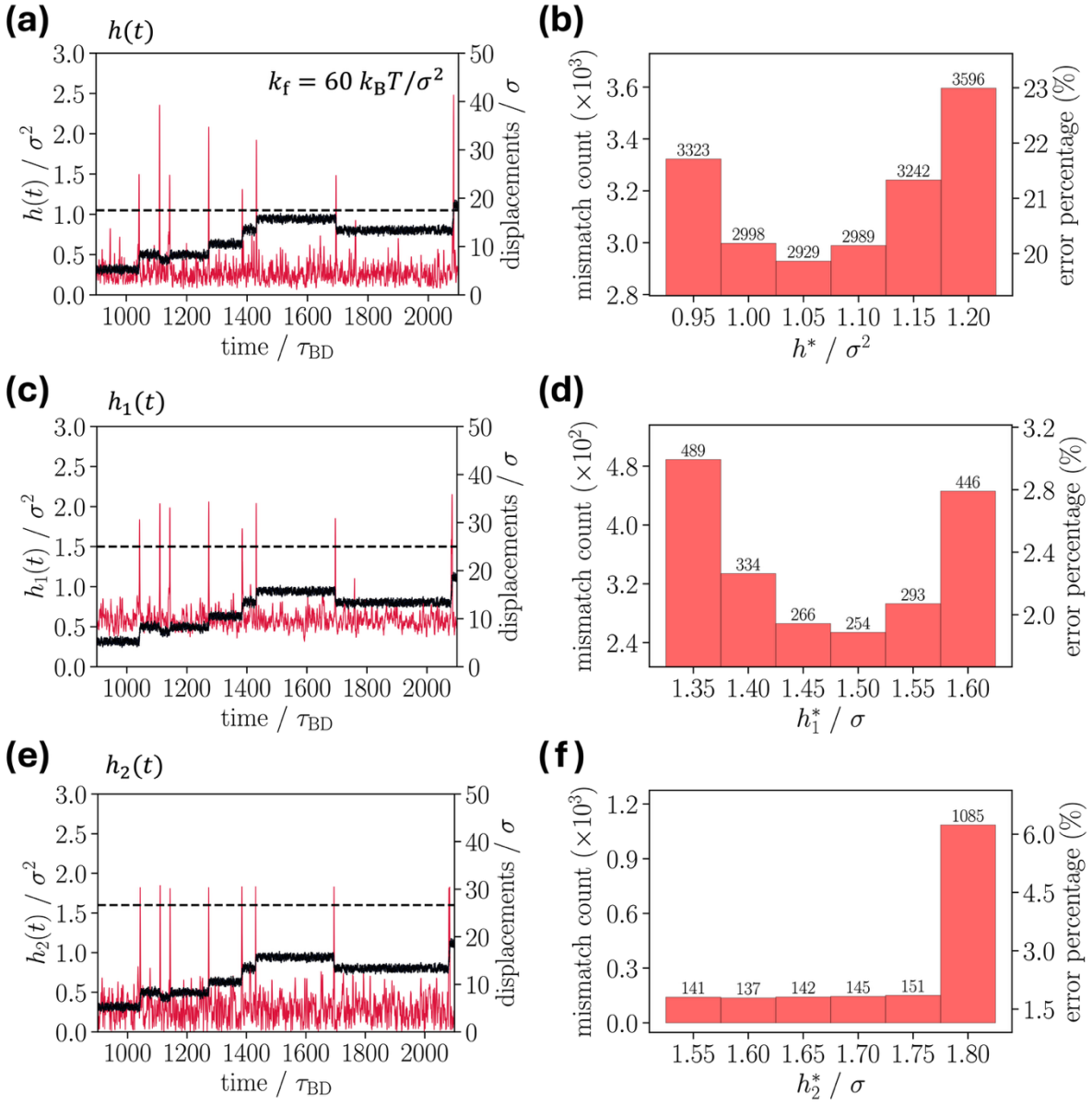

Figure S5. Validation of the hop functions for accurate identification of hopping events for $k_f = 60\ k_B T/\sigma^2$. ((a), (c), (e)) Comparisons of $h(t)$, $h_1(t)$, and $h_2(t)$ (red curves, plotted against the left y-axis) with the directly tracked tracer trajectory (black curve, plotted against the right y-axis) over the simulation period from 900 τ_{BD} to 2,100 τ_{BD} for $k_f = 60\ k_B T/\sigma^2$. Horizontal dashed lines indicate the optimized threshold values for each hop function (see Table S1), used to identify hopping events. ((b), (d), (f)) The number of inconsistent identifications of hopping events as a function of threshold values for $h(t)$, $h_1(t)$, and $h_2(t)$. The total number of hopping events directly identified from the entire simulation trajectory ($4\times10^6\ \tau_{BD}$) for $k_f = 60\ k_B T/\sigma^2$, is 15,225. The error percentage is calculated as the mismatch count divided by this total, multiplied by 100.

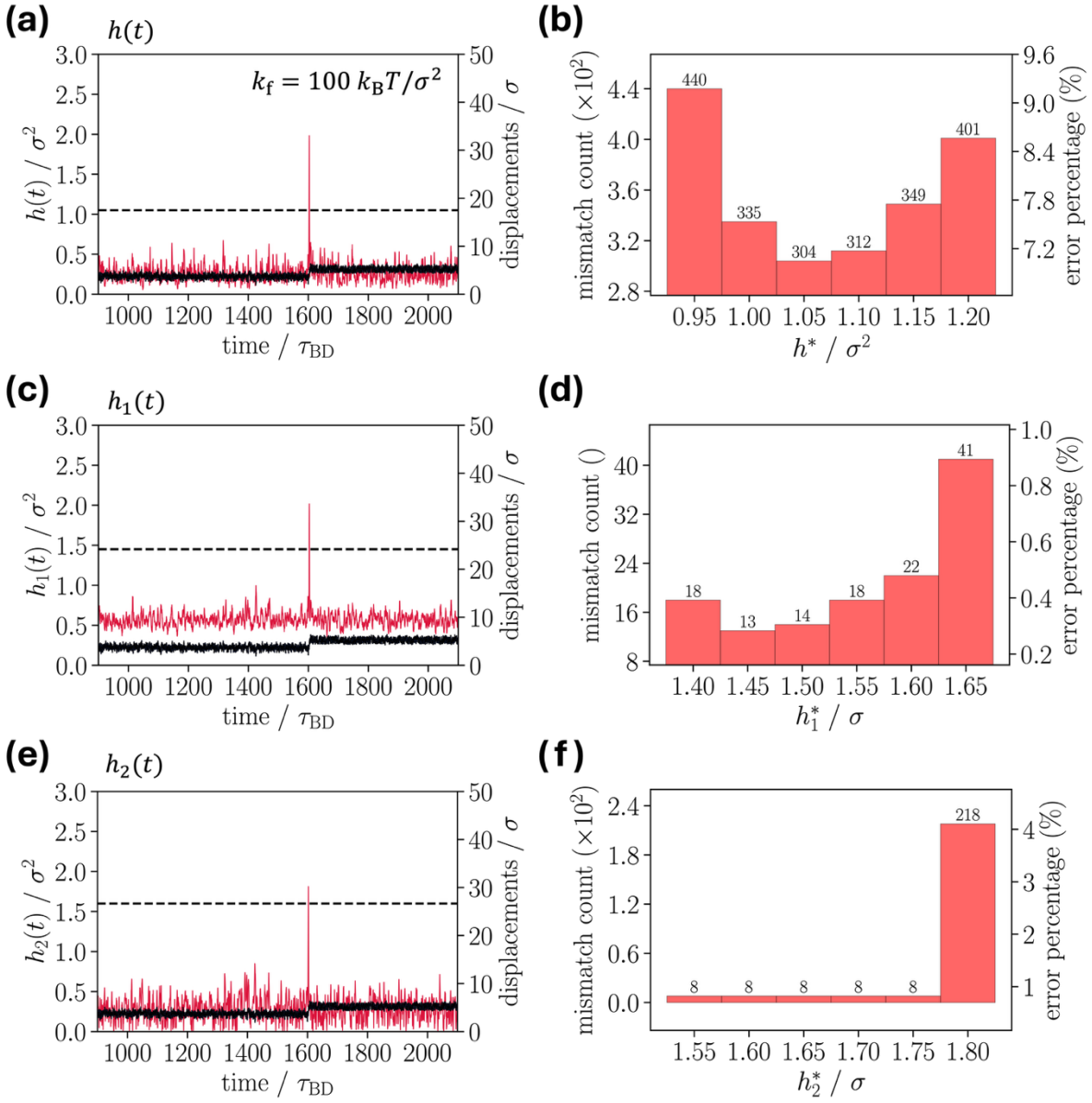

Figure S6. Validation of the hop functions for accurate identification of hopping events for $k_f = 100\ k_BT/\sigma^2$. ((a), (c), (e)) Comparisons of $h(t)$, $h_1(t)$, and $h_2(t)$ (red curves, plotted against the left y-axis) with the directly tracked tracer trajectory (black curve, plotted against the right y-axis) over the simulation period from 900 τ_{BD} to 2,100 τ_{BD} for $k_f = 100\ k_BT/\sigma^2$. Horizontal dashed lines indicate the optimized threshold values for each hop function (see Table S1), used to identify hopping events. ((b), (d), (f)) The number of inconsistent identifications of hopping events as a function of threshold values for $h(t)$, $h_1(t)$, and $h_2(t)$. The total number of hopping events directly identified from the entire simulation trajectory ($4\times10^6\ \tau_{BD}$) for $k_f = 100\ k_BT/\sigma^2$, is 4,586. The error percentage is calculated as the mismatch count divided by this total, multiplied by 100.

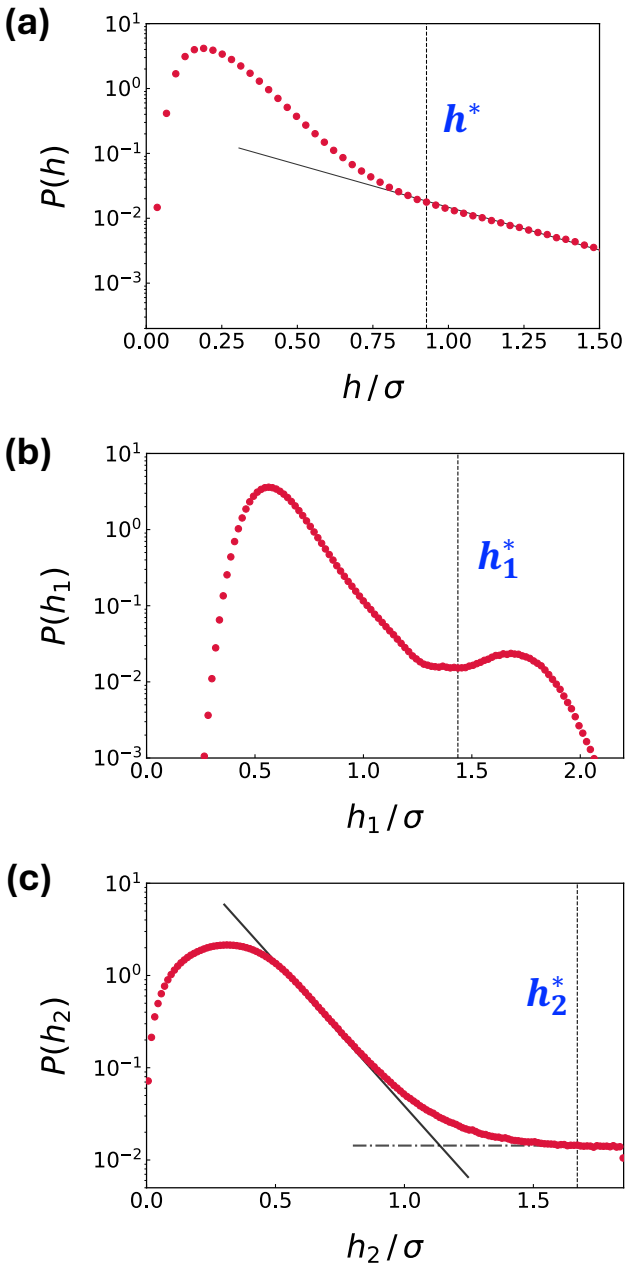

Figure S7. Probability distributions of the hop functions plotted on a semi-logarithmic scale to determine threshold values without direct tracking of hopping events for $k_f = 40\ k_B T/\sigma^2$. (a) Distribution $P(h)$ of the conventional hop function $h(t)$. The threshold h^* is determined from the onset of the exponential-tail regime beyond the Gaussian-like peak associated with caged thermal fluctuations. The solid line indicates the exponential-tail fit used to identify this regime. (b) Distribution $P(h_1)$ of the modified hop function $h_1(t)$. The threshold h_1^* is determined from the local minimum between the main caged-motion peak and the secondary hopping-related peak. (c) Distribution $P(h_2)$ of the modified hop function $h_2(t)$. The threshold h_2^* is determined from the onset of the plateau-like regime, where the contribution from hopping configurations becomes dominant over the exponentially decaying caged-fluctuation contribution. The solid line indicates the exponential decay of the caged contribution, and the dash-dotted line indicates the plateau-like contribution. Vertical dashed lines mark the resulting threshold values.

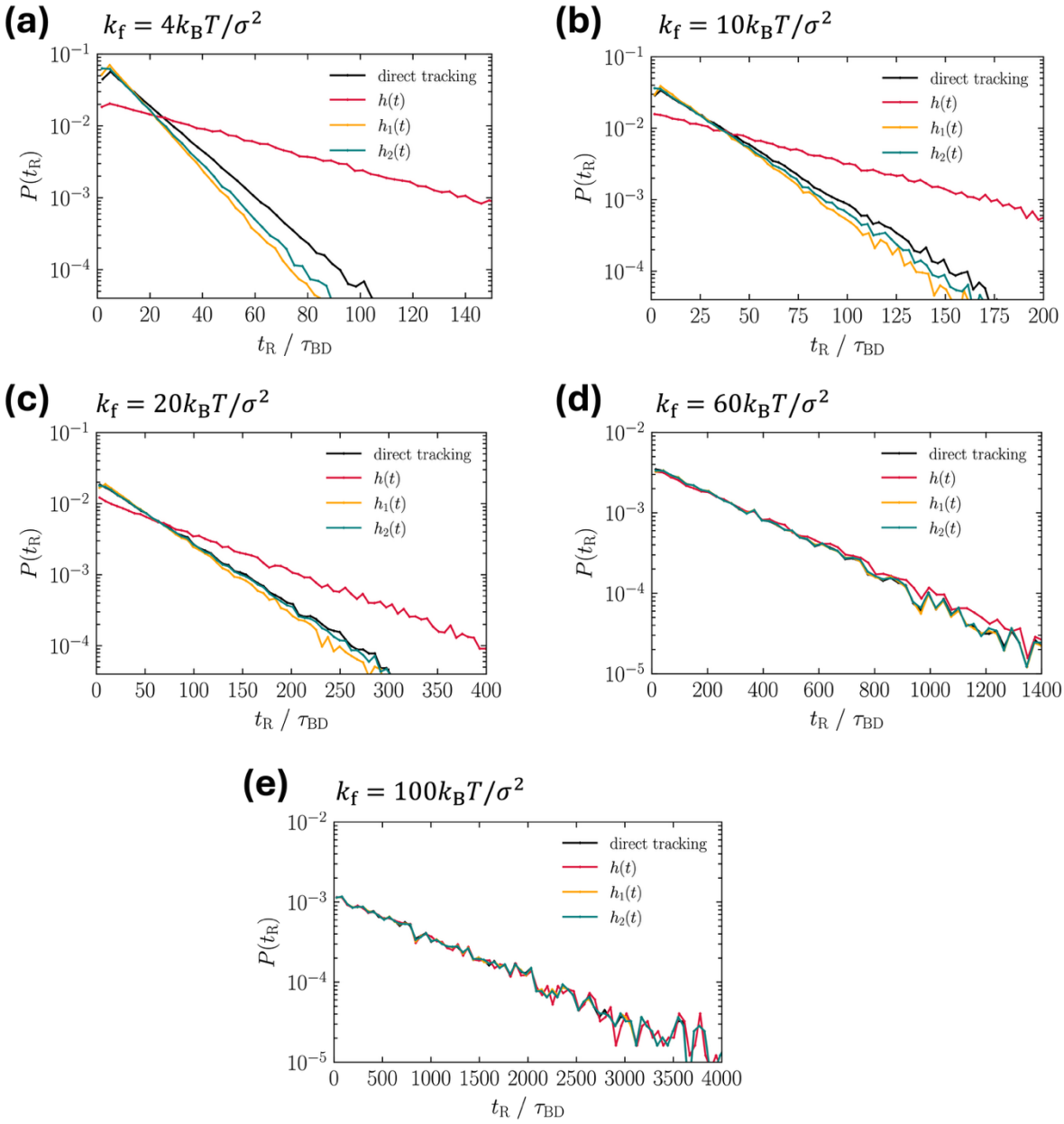

Figure S8. Probability distribution of the residence time, t_R, defined as the time interval between consecutive hopping events of $h(t)$, $h_1(t)$, and $h_2(t)$, compared with that from direct tracer tracking. Data are shown for (a) $k_f = 4$, (b) 10, (c) 20, (d) 60, and (e) 100 k_BT/σ^2.

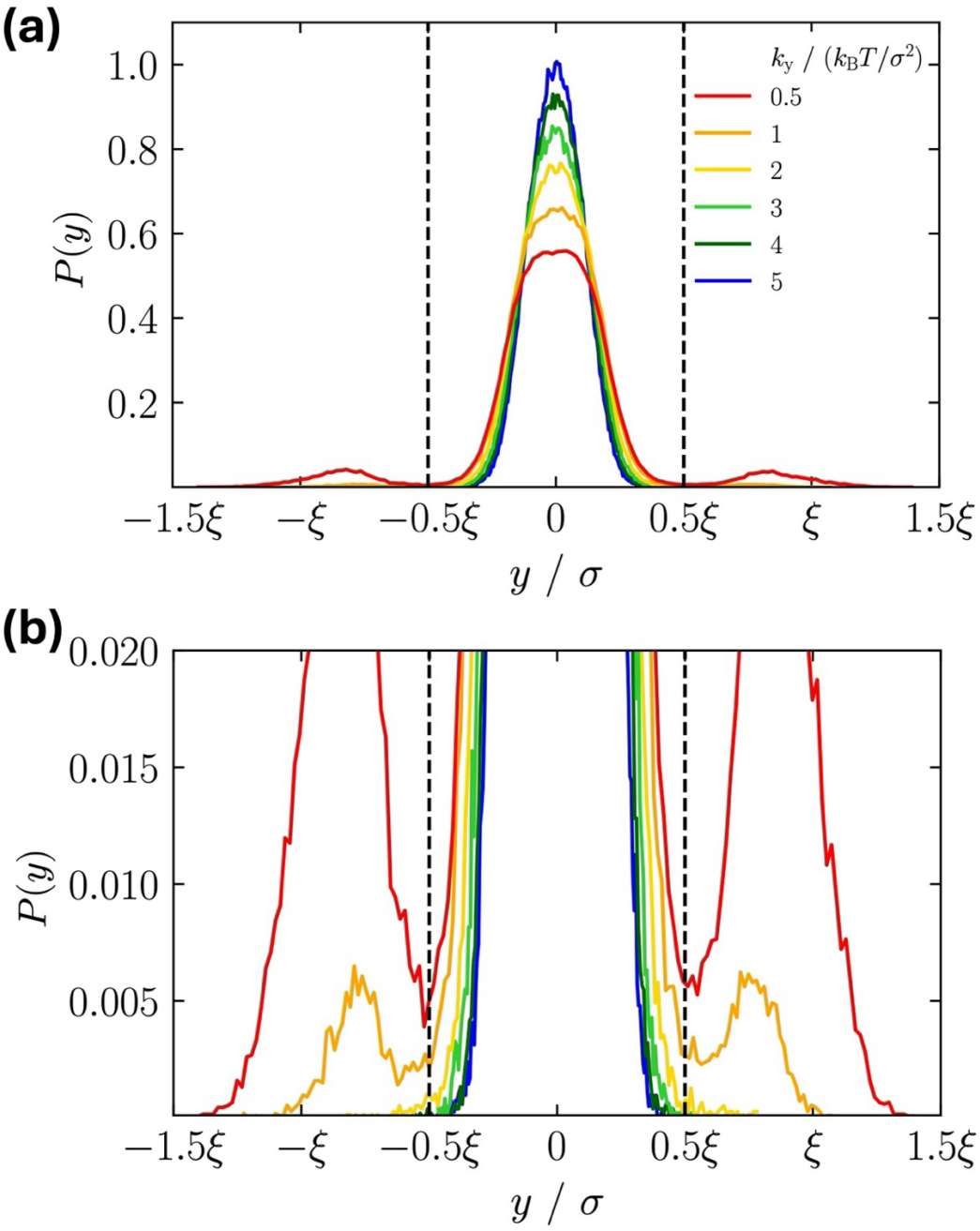

Figure S9. Comparison of the distribution of the tracer along the y-direction for the restraining constant k_y= 0.5, 1, 2, 3, 4 and 5 k_BT/σ^2 at $x = 0$. (a) Probability distributions $P(y)$ along the y-direction. ξ is the mesh size. (b) Magnified view of the probability distributions. When $k_y \geq 3\ k_BT/\sigma^2$, the tracer remains confined within $-\xi/2 \leq y \leq \xi/2$, corresponding to a region inside a single lattice site. This confinement ensures that, during umbrella sampling, where the tracer is pulled along the x-axis, the tracer does not drift into neighboring lattices in the y-direction. These data were obtained for the lattice with $k_f = 40\ k_BT/\sigma^2$.

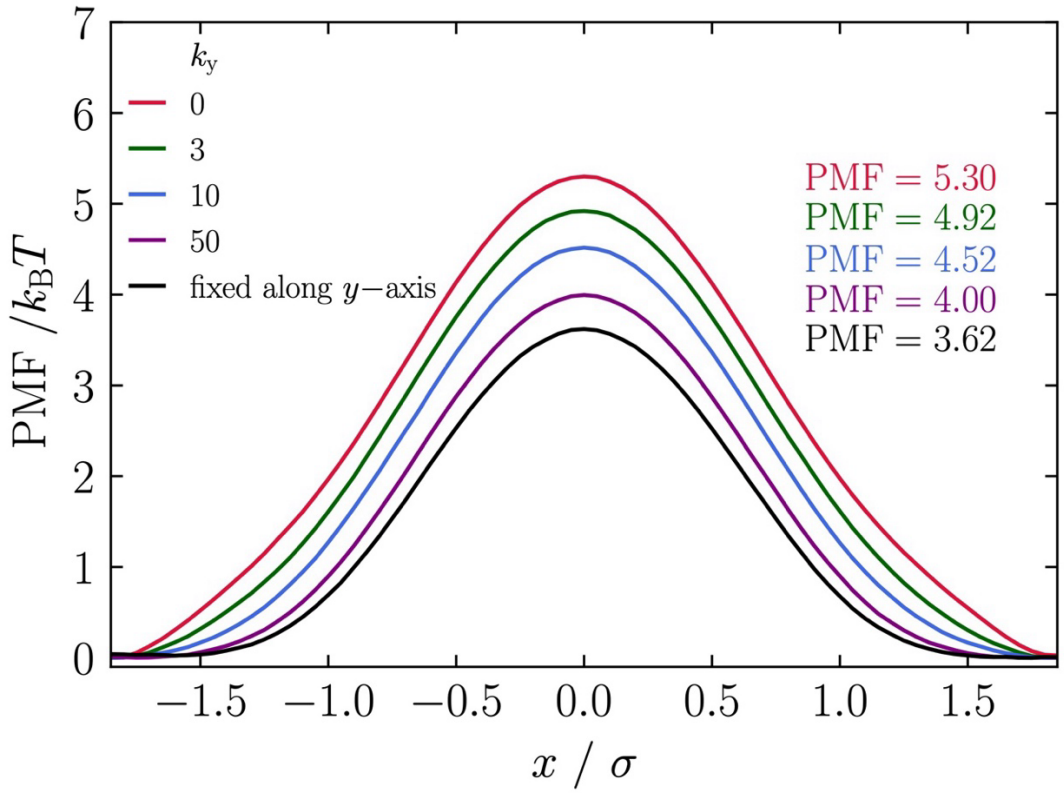

Figure S10. Comparison of the potential of mean force (PMF) profiles of the tracer along the x-axis under different restraining conditions: free along the y-axis ($k_y = 0$), restrained along the y-axis with the y-directional force constant of k_y= 3, 10, 50 k_BT/σ^2, and fixed along y-axis. We present the PMF result using k_y= 3 k_BT/σ^2 in the main text to prevent the tracer from drifting into the neighboring interstitial regions while allowing small fluctuations along the y-direction. These data were obtained for the lattice with k_f = 40 k_BT/σ^2.

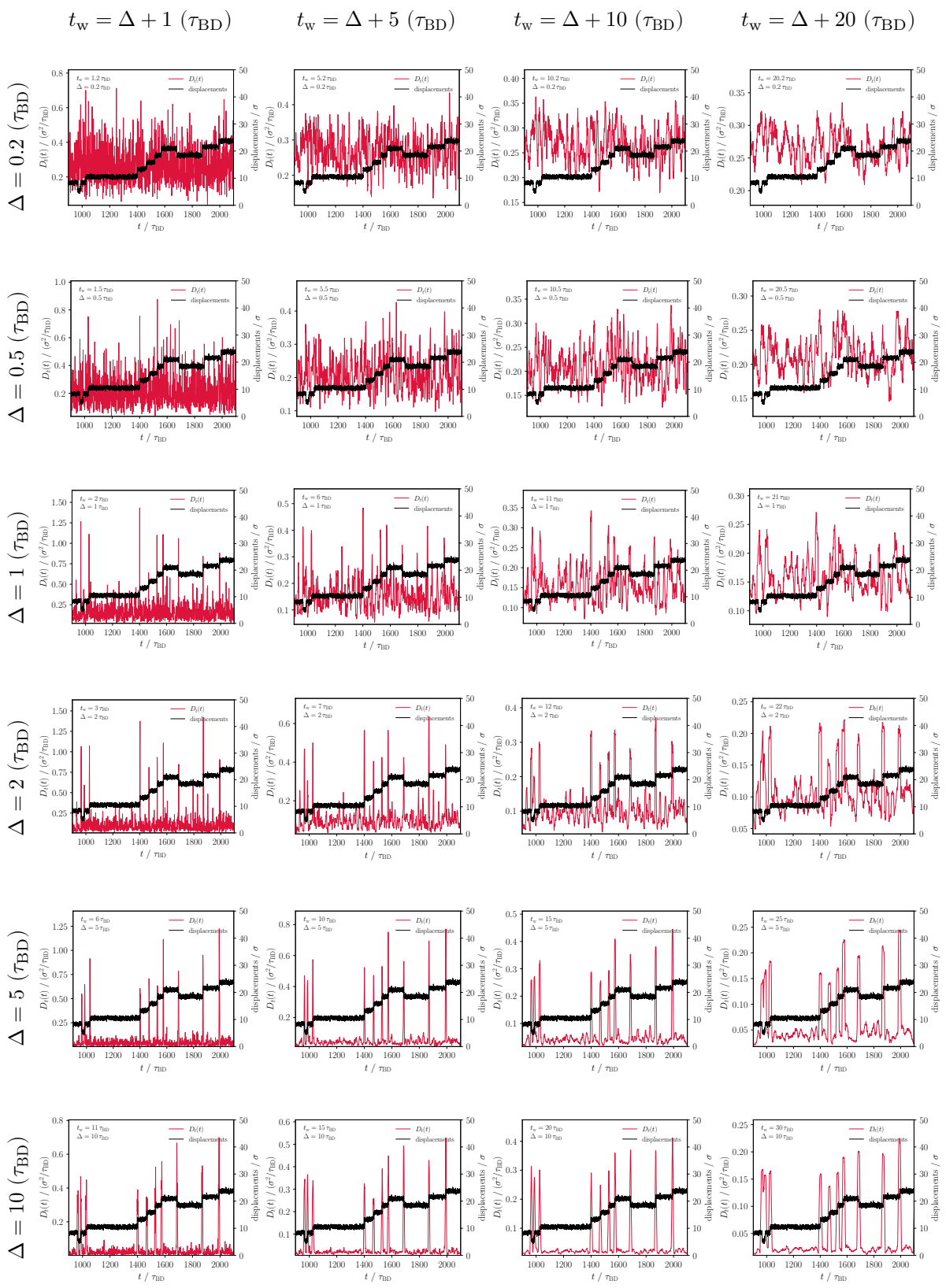

Figure S11. Comparisons of the time-local diffusion coefficient $D_t(t)$ with the directly tracked tracer trajectory for various combinations of the lag time Δ and the analysis window t_w at $k_f = 40\, k_B T/\sigma^2$. Each panel shows $D_t(t)$ (red curve, plotted against the left y-axis) and the directly tracked tracer trajectory (black curve, plotted against the right y-axis) over the simulation period from 900 τ_{BD} to 2,100 τ_{BD}. The rows correspond to different lag

times (top to bottom: $\Delta = 0.2, 0.5, 1, 2, 5, 10\ \tau_{\mathrm{BD}}$), and the columns correspond to different analysis windows defined as $t_{\mathrm{w}} = \Delta + \tau_{\mathrm{off}}$(left to right: $\tau_{\mathrm{off}} = 0.2$,0.5,1,5,10,20 τ_{BD}); the resulting (Δ, t_{w})values are indicated in the upper-left corner of each panel. Smaller Δ yields a noisier $D_t(t)$ signal sensitive to short-time fluctuations, whereas larger Δ smooths the signal and accentuates hopping events that coincide with sharp steps in the displacement trajectory. The combination $(\Delta, t_{\mathrm{w}}) = (5,6)\ \tau_{\mathrm{BD}}$, used in the main text for D_t-based identification of hopping events, balances peak prominence with temporal resolution.

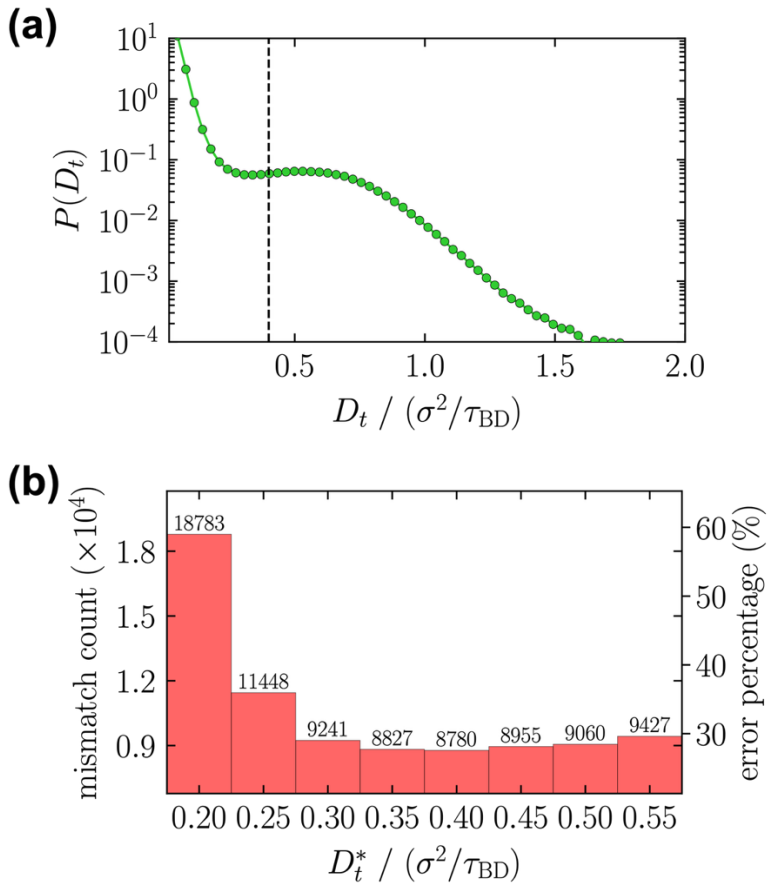

Figure S12. Validation of the time-local diffusion coefficient $D_t(t)$ for accurate identification of hopping events at $k_f = 40\, k_B T/\sigma^2$. (a) Probability density $P(D_t)$ of $D_t(t)$ computed with $\Delta = 5\,\tau_{BD}$ and $t_w = \Delta + 1 = 6\,\tau_{BD}$, accumulated from all 40 independent sample trajectories at $k_f = 40\, k_B T/\sigma^2$. The vertical dashed line marks the optimized threshold $D_t^* = 0.40\,\sigma^2/\tau_{BD}$ used to identify hopping events. (b) Number of inconsistent identifications of hopping events as a function of the threshold D_t^* for $(\Delta, t_w) = (5,6)\,\tau_{BD}$. The mismatch count attains a clear minimum at $D_t^* = 0.40\,\sigma^2/\tau_{BD}$, with 8,780 inconsistent identifications. As in Figure 3 of the main text, the total number of hopping events directly identified from the entire simulation trajectory ($4 \times 10^6\,\tau_{BD}$) for $k_f = 40\, k_B T/\sigma^2$is 31,839, and the error percentage is defined as the mismatch count divided by this total, multiplied by 100.

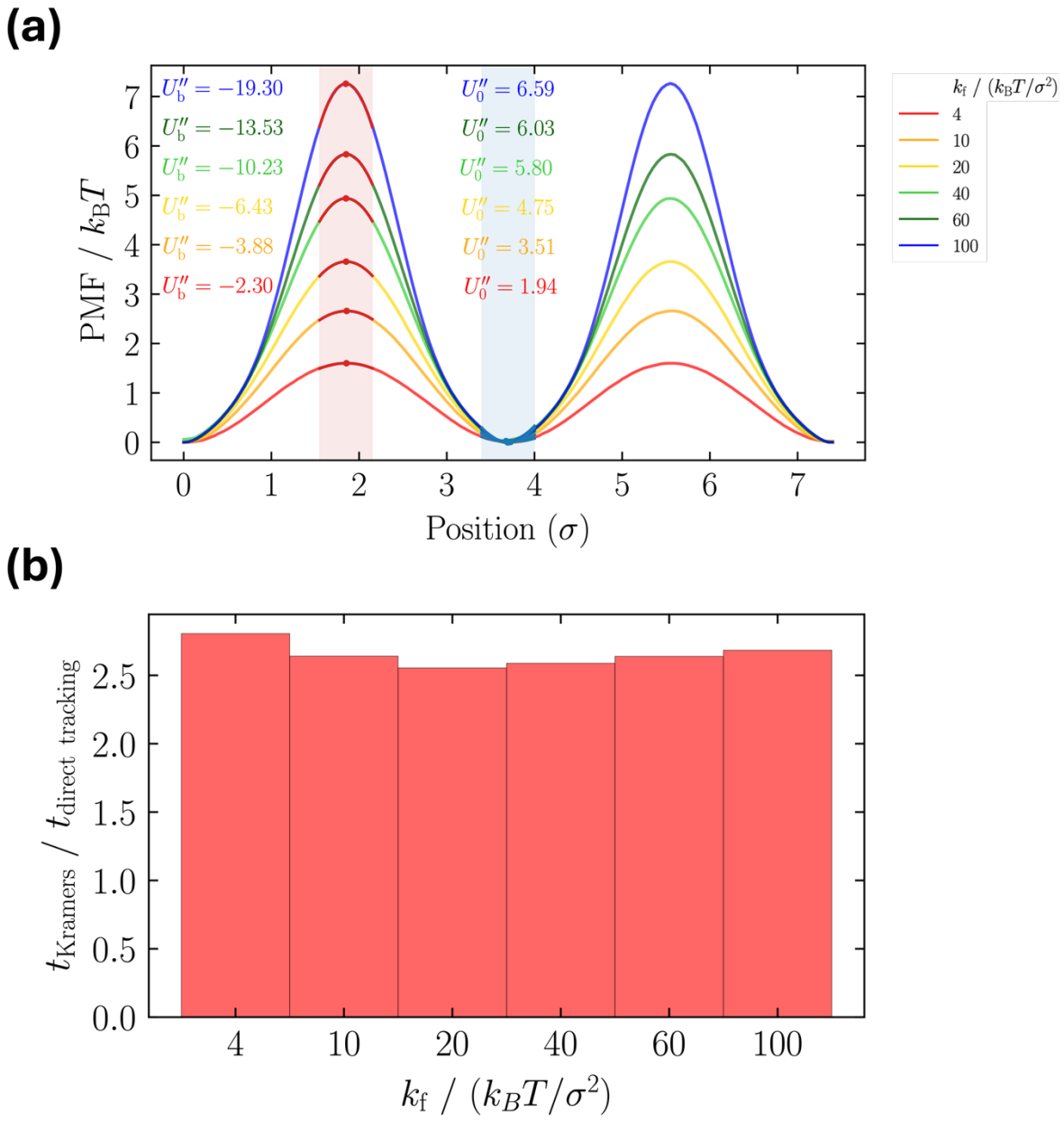

Figure S13. Calculation of residence time using Kramers' theory. (a) Local curvatures U_0'' and U_b'' obtained from umbrella-sampling PMF profiles for $k_f = 4$, 10, 20, 40, 60, and 100 k_BT/σ^2. The fitting was performed within a local window of width 0.6 σ. The qualitative conclusion remains unchanged regardless of the choice of window width. The red window near the barrier ($x = 1.85\ \sigma$) is fitted to the equation $U_b(x) = c_0 + c_1(x - 1.85) + \frac{1}{2}c_2(x - 1.85)^2$ where $c_2 = U_b''$. Similarly, the blue window near the well ($x = 3.7\ \sigma$) is fitted to the equation $U_0(x) = c_0 + c_1(x - 3.7) + \frac{1}{2}c_2(x - 3.7)^2$ where $c_2 = U_0''$. (b) Ratio between the residence time obtained from Kramers' theory to that from direct tracking, showing that $t_{Kramers}/t_{direct\ tracking} \approx 2.5$.